Preprint

SiliconPV 2024

Minimizing critical materials for contacting cells and modules

https://doi.org/10.52825/xxxx........ DOI placeholder (WILL BE FILLED IN BY TIB Open Publishing)

© Authors. This work is licensed under a Creative Commons Attribution 4.0 International License

Published: (WILL BE FILLED IN BY TIB Open Publishing)

PECVD Si_xC_y as Barrier Layer against Aluminum in Solar Cells with poly-Si/SiO_x Passivating Contacts

David Bäurle[1] [https://orcid.org/0009-0001-8571-885X], Benjamin Gapp[1] [https://orcid.org/0000-0002-4620-977X], Giso Hahn[1] [https://orcid.org/0000-0001-8292-1281], Heiko Plagwitz[1] [https://orcid.org/0000-0003-2869-0149], and Barbara Terheiden[1]

[1] University Konstanz, Germany

*Correspondence: David.baeurle@uni-konstanz.de

Abstract. We investigate the barrier properties of phosphorus-doped Si-rich silicon carbide (Si_xC_y) thin films deposited by PECVD against Al/Si alloying in the context of poly-Si/SiO_x passivating contacts. The stability of the implied open circuit voltage (iV_{OC}) after firing of single-sided, full area screen-printed Al-contacts increases with carbon content of the barrier layer and depends on the crystallization scheme applied to the samples. Crystallized Si_xC_y layers with an atomic C concentration of about 20 at.% deposited on pre-crystallized poly-Si predominantly show no significant decrease in iV_{OC} values for peak firing temperatures up to 725°C.

Keywords: Passivating contacts, Metallization, Aluminum, Silicon carbide

1. Introduction

Solar cells with a passivating contact, based on poly-Si and a thin SiO_x layer, show high efficiencies beyond η = 26% due to their excellent charge carrier selectivity and passivation quality under the metal contacts [1, 2]. Ag serves usually as contact metal. However, the availability of expensive materials as Ag becomes limiting for a terawatt scale production [3]. Therefore, alternatives to Ag are needed. Al metallization is such an approach. The drawback of Al in this context is the strong alloying with silicon that would dissolve the poly-Si/SiO_x contact completely. The introduction of a barrier layer with sufficiently high conductivity between poly-Si and Al metallization is the solution investigated in this contribution. Different phosphorus-doped Si-rich Si_xC_y thin films deposited by plasma-enhanced chemical vapour deposition (PECVD) are studied regarding their barrier properties against Al.

2. Experimental

For this work, n-type (42 and 18 Ωcm) Cz-Si wafers with a size of 156.75x156.75 mm^2 and a thickness of 150 µm were saw damage etched by KOH. Afterwards, the samples underwent wet chemical cleaning processes. A thin SiO_x layer (~1.7 nm) was grown by thermal oxidation in a tube furnace. Subsequently, 100 nm of phosphorus-doped amorphous silicon ((n) a-Si) were deposited by PECVD. The samples were cut to a size of 50x50 mm^2 and subjected to different crystallization schemes, Figure *1*. For samples of group A and B the (n) a-Si was pre-crystallized in a tube furnace at 920°C before 50 nm of amorphous phosphorus-doped PECVD (n) a-Si_xC_y were deposited by using the precursors SiH_4, CH_4 and PH_3. A second temperature treatment at 920°C was applied to group B to additionally crystallize the (n) Si_xC_y layer. Samples of group C were exposed to one combined crystallization step after depositing (n) a-Si_xC_y

onto the uncrystallized (n) a-Si. An overview of the crystallization schemes and sample composition is given in Figure *1*.

To investigate the influence of the high temperature anneal on the Si_xC_y layers we performed Fourier-transform infrared spectroscopy (FTIR) measurements to analyze the occurring bonds. Therefor we deposited the thin films on chemically polished FZ-Si.

The (n) a-Si_xC_y deposition was carried out with varying CH_4 gas flow to adjust the carbon content whereas the other process conditions were kept constant. In the following the relation between CH_4 and SiH_4 gas flow (*R*) will be stated to identify the different samples. To quantify the carbon content, SIMS (secondary ion mass spectrometry) measurements were performed on selected samples.

Figure 1. Process flow of the different crystallization schemes and the cross section of a typical sample.

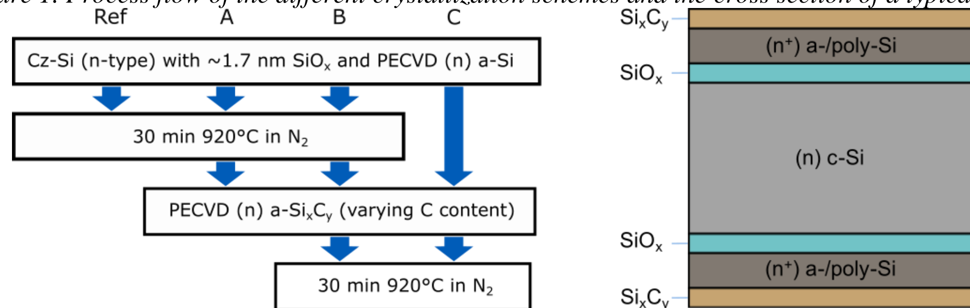

Figure 1. *Process flow of the different crystallization schemes and the cross section of a typical sample.*

To examine the different barrier layers, the samples were single-sided full area screen-printed with Al-paste and fired in a conventional belt furnace. The measured peak temperatures, using a thermocouple, ranged between T_{Peak} = 675-750°C with a measurement uncertainty of ±10°C.The barrier layer functionality was evaluated by comparing the iV_{OC} values of the samples before screen-printing the Al-paste and after metallization and removal of Al in aqueous HCl. Photoconductance decay (PCD) measurements to determine iV_{OC} were performed using a Sinton lifetime tester.

3. Results and Discussion

3.1 Crystallization schemes

The high temperature anneal leads to various changes in the Si_xC_y thin films. Measurements with FTIR show that bonds are reorganized, **Fehler! Verweisquelle konnte nicht gefunden werden.**(i). In the as-deposited a-Si_xC_y:H films Si-H_n and C-H_n bonds could be detected. The absorption band at 2070 cm^{-1} can by assigned to the Si-$H_{1,2}$ stretching vibration [4]. Between 2800 cm^{-1} and 3000 cm^{-1} C-H_n stretching vibrations cause weak absorption bands [5, 6]. In the crystallized Si_xC_y films those hydrogen bonds are not detected anymore which indicates an effusion of hydrogen during the high temperature anneal. Si-C stretching vibrations lead to an absorption band between 760 cm^{-1} and 800 cm^{-1} [5-7]. In this range the absorption increases strongly after the crystallization which indicates that Si-C bonds are formed. An increasing absorption can also be observed around 1070 cm^{-1}. This can be assigned to various silicon and oxygen related bonds [8, 9]. Those Si-O_x bonds are presumably formed at the surface, after the sample re-enters ambient air at a temperature of 800°C.

Another indication for this oxidation after crystallization can be seen in the glow-discharge optical emission spectroscopy (GD-OES) profiles of layer stacks processed after crystallization scheme B and C. In **Fehler! Verweisquelle konnte nicht gefunden werden.** (ii), the profile of sample B shows an increased oxygen signal between the poly-Si and the Si_xC_y

layer which is not observed in sample C where no pre-crystallization of the a-Si was performed. The poly-Si can be identified between the onset of the carbon signal (Si_xC_y layer) and the small oxygen signal at 13 s which corresponds to the thin interfacial SiO_x.

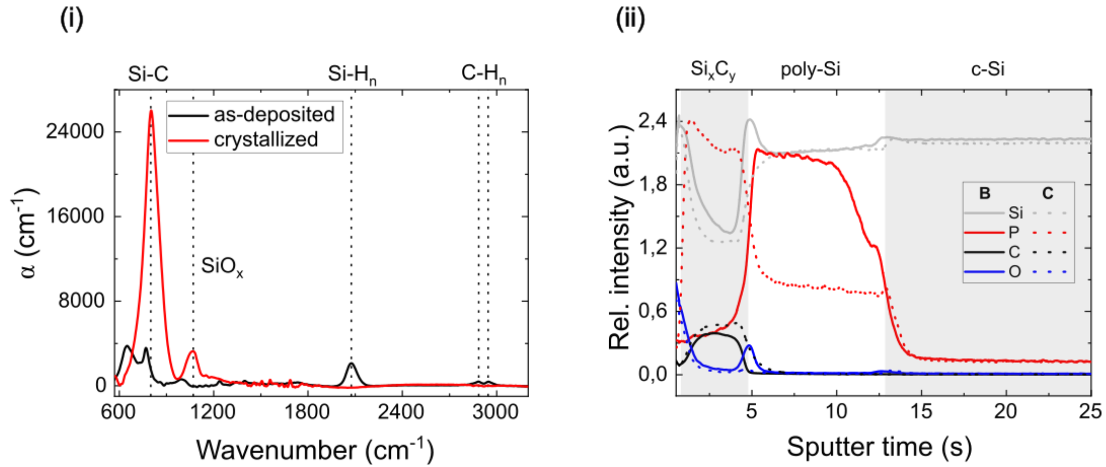

Figure 2. (i) *Absorption spectrum of the Si_xC_y layer before and after the high temperature anneal recorded via FTIR.* (ii) *GD-OES profile of samples crystallized after scheme B and C.*

The additionally arising SiO_x in crystallization scheme B seems to be a diffusion barrier for the phosphorus in the poly-Si. In the sample with the additional SiO_x the P signal in the poly-Si is significantly stronger than in the Si_xC_y and c-Si. Whereas for the sample of group C the phosphorus seems to diffuse into the Si_xC_y layer. Here the P signal is considerably higher in the Si_xC_y layer than in the poly-Si.

Furthermore, it was analyzed how the crystallization scheme impacts the passivation quality. As seen in Figure 3, the initial iV_{OC} values vary strongly with the applied sample preparation. Samples of group A show even without further hydrogenation an iV_{OC} values up to 731 mV. The crystallization of the Si_xC_y layers and the associated changes appear to deteriorate the surface passivation. In groups B and C, the initial iV_{OC} values are limited to 698 mV or 685 mV respectively. If those samples are exposed to a hydrogenation by the deposition of an additional hydrogen-rich SiN_x layer and a subsequent fast firing step, the passivation of groups B and C improve significantly. After hydrogenation all samples show excellent surface passivation with iV_{OC} values in the range of 721-731 mV.

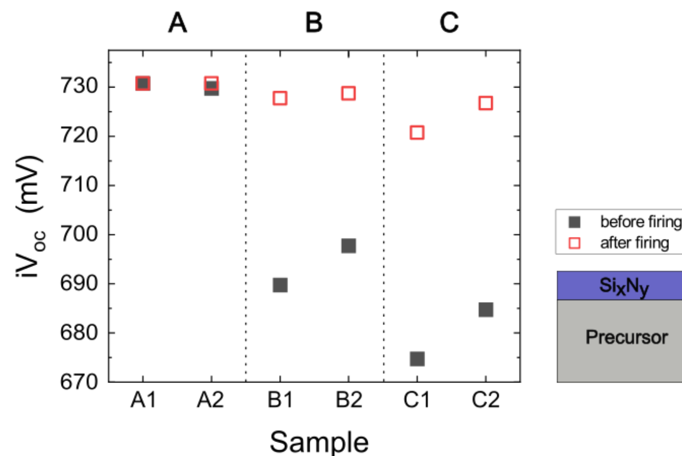

Figure 3. *iV_{OC} measurements of unmetallized samples processed after the different crystallization schemes before and after hydrogenation with SiN_x and fast firing. The precursor shown in the schematic sample cross section equals the cross section illustrated in Figure 1.*

3.2 Barrier functionality

The influence of crystallization scheme and carbon content on the barrier functionality of Si_xC_y layers is shown in Figure 4 (i) for samples of group A, B and C without hydrogenation. All represented samples were fired at a measured T_{Peak} = 675°C. SIMS measurements indicate that the carbon content for an increasing R = 3-6 rises from around 10 to 20 at.%. Compared to the reference sample without barrier layer, samples of group A and B show significantly higher iV_{OC} values after metallization and subsequent etch-back.

In particular, for samples with as-deposited barrier layers (group A) the carbon content seems to increase the stability of the iV_{OC} after metallization. In Group A an initial iV_{OC} up to 722 mV is achieved. After full-area metallization and etch-back, the iV_{OC} of the sample with the a-Si_xC_y layer with maximum carbon content is 711 mV. The loss in iV_{OC} indicates a decreasing barrier functionality.

The second crystallization which is performed on samples of group B limits the initial iV_{OC} to values of around 700 mV without hydrogenation. Nevertheless, those samples of group B show highest stability regarding iV_{OC} after metallization with no shown decrease in the tested temperature range. As shown in the previous section, it is expected that an additional hydrogenation can overcome the limitation in the initial iV_{OC}. This makes the shown barrier functionality of group B most promising.

The combined crystallization of (n) a-Si and (n) a-Si_xC_y applied in group C leads to samples with inferior barrier functionality. Only for the sample with highest carbon content the iV_{OC} value after metallization and etch-back is higher than that of the reference sample without any barrier layer, shown in Figure 4 (i).

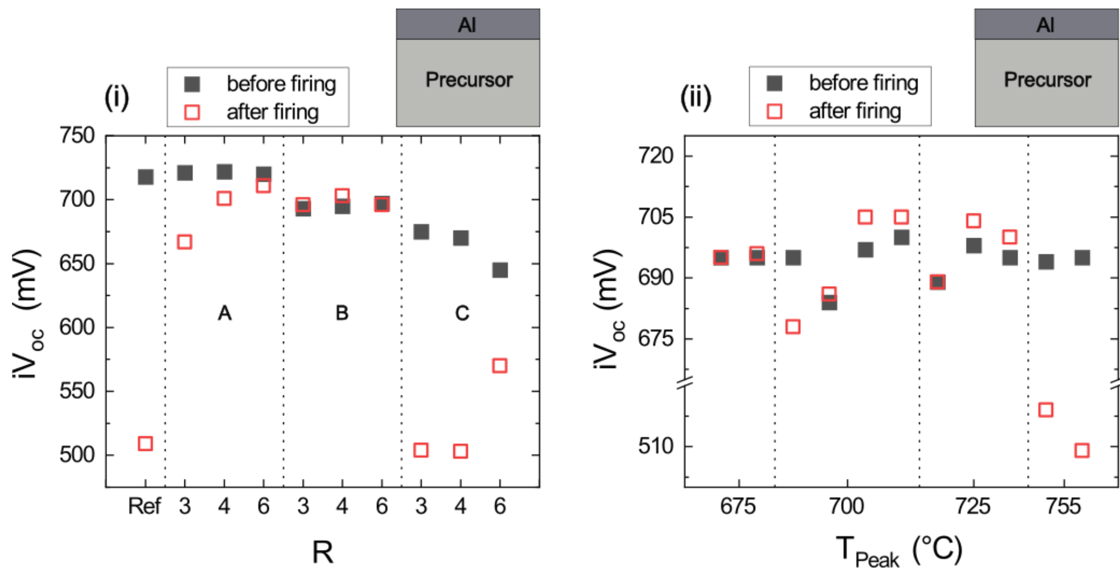

Figure 4. (i) *iV_{oc} measurements, before metallization and after metallization with subsequent etch-back, of samples (42 Ωcm) processed with varying crystallization scheme (A/B/C) and CH_4/SiH_4 ratio R fired at T_{Peak} = 675°C.* ***(ii)*** *iV_{oc} measurements, before metallization and after metallization with subsequent etch-back, of samples (18 Ωcm) with R = 6 and crystallization scheme B, fired at varying measured T_{Peak}. The precursor shown in the schematic sample cross sections equals the cross section illustrated in Figure 1.*

To further investigate the barrier functionality, a variation of the peak firing temperature was performed on samples which were crystallized following scheme B and featuring Si_xC_y layers with maximum carbon content. The stability of iV_{OC} values depending on T_{Peak} is illustrated in **Fehler! Verweisquelle konnte nicht gefunden werden.**(ii). Except for one sample

the iV_{OC} is not decreasing during metallization for temperatures up to T_{Peak} = 725°C. The iV_{OC} of some samples even shows a small increase of up to 8 mV. Firing the samples at T_{Peak} = 755°C dissolves the poly-Si/SiO_x passivating contact completely which results in iV_{OC} values below 520 mV, which is comparable to the reference sample without barrier layer.

4. Conclusion

The ability of different PECVD Si_xC_y layers to prevent aluminum from dissolving the poly-Si/SiO_x passivating contact depends on both the crystallization scheme during sample preparation and the carbon content. The impact of the carbon content is mainly visible for samples with as-deposited barrier layers (group A). Here, the barrier functionality increases significantly with an increasing carbon content from 13.5(23) to 19.3(23) at.%. A pre-crystallization of the a-Si before depositing the Si_xC_y seems to be even more important. Samples with one simultaneous crystallization (group C) show basically no barrier functionality compared to reference samples without barrier layer. Annealed Si_xC_y layers which were deposited on pre-crystallized poly-Si (group B) exhibit the most promising barrier properties. For peak firing temperatures up to 725°C those sample show predominantly no decrease in iV_{OC} after metallization with Al and subsequent Al removal.

Data availability statement

The data that support the findings of this study are available from the corresponding author upon reasonable request.

Author contributions

D. Bäurle: formal analysis, investigation, validation, visualization, conceptualization, writing – original draft; **B. Gapp**: conceptualization, validation; **G. Hahn**: supervision, writing – review & editing; **H. Plagwitz**: conceptualization, validation, supervision, project administration; **B. Terheiden**: conceptualization, supervision, funding acquisition, project administration, writing – review & editing

Competing interests

The authors declare that they have no competing interests.

Funding

Part of this work was financially supported by the German Federal Ministry for Economic Affairs and Climate Action (FKZ 03EE1106B). The content is the responsibility of the authors.

Acknowledgement

The authors would like to thank Thomas Pernau for the a-Si depositions.

References

[1] F. Haase, C. Hollemann, S. Schäfer, A. Merkle, M. Rienäcker, J. Krügener, R. Brendel, and R. Peibst, "Laser contact openings for local poly-Si-metal contacts enabling 26.1%-efficient POLO-IBC solar cells", Sol. Energy Mater. Sol. Cells, vol.186, pp. 184-193, Nov., 2018, doi: https://doi.org/10.1016/j.solmat.2018.06.020.

[2] A. Richter, R. Müller, J. Benick, F. Feldmann, B. Steinhauser, C. Reichel, A. Fell, M. Biv our, M. Hermle, and S. W. Glunz, "Design rules for high-efficiency both-sides-contacted silicon solar cells with balanced charge carrier transport and recombination losses", Nat. Energy, vol.6, no.4, pp. 429-438, Apr., 2021, doi: https://doi.org/10.1038/s41560-021-00805-w.

[3] Y. Zhang, M. Kim, L. Wang, P. Verlinden, and B. Hallam, "Design considerations for multi-terawatt scale manufacturing of existing and future photovoltaic technologies: challenges and opportunities related to silver, indium and bismuth consumption", Energy Environ. Sci., vol.14, no.11, pp. 5587-5610, Nov., 2021, doi: https://doi.org/10.1039/D1EE01814K.

[4] [26] K.M. McNamara, B.E. Williams, K.K. Gleason, and B.E. Scruggs, "Identification of defects and impurities in chemical-vapor-deposited diamond through infrared spectroscopy", J. Appl. Phys., vol. 76, no. 4, Aug., 1994, doi: https://doi.org/10.1063/1.357598.

[5] P.I. Rovira, and F. Alvarez, "Chemical (dis)order in a-$Si_{1-x}C_x$:H for x<0.6", Phys. Rev. B, vol.55, no.7, pp. 4426-4434, Feb., 1997, doi: https://doi.org/10.1103/PhysRevB.55.4426.

[6] T. Friessnegg, M. Boudreau, P. Mascher, A. Knights, P.J. Simpson, and W. Puff, "Defect structure of carbon rich a-SiC:H films and the influence of gas and heat treatments", J. Appl. Phys., vol. 84, no. 2, Jul., 1998, doi: https://doi.org/10.1063/1.368138.

[7] N.V. Tzenov, M.B. Tzolov, and D.I. Dimova-Malinovska, "Hydrogen-assisted surface reactions during the growth of sputtered a-SiC:H films", Semicond. Sci. Technol., vol. 9, no. 1, pp. 91-96, Jan., 1994, doi: https://doi.org/10.1088/0268-1242/9/1/016.

[8] Z. An, R.K.Y. Fu, P. Chen, W. Liu, P.K. Chu, and C. Lin, "Silicon carbide formation by methane plasma immersion ion implantation into silicon", J. Vac. Sci. Technol. B, vol.21, no.4, pp. 1375-1379, Jul., 2003, doi: https://doi.org/10.1116/1.1591741.

[9] M. Künle, T. Kaltenbach, P. Löper, A. Hartel, S. Janz, O. Eibl, and K-G. Nickel, "Si-rich a-SiC:H thin films: Structural and optical transformations during thermal annealing", Thin Solid Films, vol.519, no.1, pp. 151-157, Oct., 2010, doi: https://doi.org/10.1016/j.tsf.2010.07.085.